Underwater quantitative thickness mapping through marine growth for corrosion measurement using shear wave EMAT with high lift-off performance

Peng Zuo*

*Advanced Remanufacturing & Technology Centre (ARTC), Agency for Science, Technology and Research (A*STAR), 3 Cleantech Loop, #01/01 CleanTech Two, Singapore, 637143, Republic of Singapore*

Abstract

Underwater inspection is important to ensure the safety, integrity and functionality of underwater structures. Although numerous conventional methods have been adopted for underwater inspection, successful application of most methods relies on the surface condition of the object, which, however, is typically covered by marine growth. Consequently, routine inspection requires thorough cleaning of marine growth, which is time-consuming and costly. Hence a method which can inspect objects without the need for extensive surface cleaning is necessary. Two methods have the potential to achieve this: pulse eddy current (PEC) and electromagnetic acoustic transducer (EMAT). PEC attains a significant lift-off distance, enabling inspection through marine growth. However, it suffers from high sensitivity to environmental conditions and low inspection accuracy due to 'relative' property which means its results are interpreted by comparing received signals to reference values. In contrast to PEC, EMAT provides 'absolute' measurements, ensuring precise results in the inspection. But it is limited by a small lift-off distance ($< 2\sim3$ mm), rendering it unsuitable for underwater applications with marine growth. Therefore, if the lift-off distance can be enhanced to a specific value, this method may offer a superior solution for underwater inspections. In this paper, a quantitative measurement method is proposed through employing a shear wave EMAT with high lift-off performance. A repelling configuration of magnets is introduced to achieve a significantly improved maximum effective lift-off distance of up to 5 mm in both air and seawater conditions with only 400 Vpp applied. This EMAT is then demonstrated to measure thickness through marine growth, showing excellent underwater performance in quantitative thickness mapping for corrosion inspection.

Keywords: Underwater corrosion measurement, Quantitative thickness mapping, Marine growth, Shear wave EMAT, High lift-off performance

1. Introduction

Underwater nondestructive inspection is a process of examining the condition of underwater structures (such as offshore structures, underwater pipelines and naval vessels). This process is of importance for ensuring the safety, integrity and functionality of these structures, as they are vulnerable to cracks and corrosion, the most common types of damage, which may easily cause weight-loss or thickness thinning, resulting in structure failure and catastrophic outcomes [1]. Because of the harsh conditions in the submarine environment, underwater inspection is typically performed by trained divers or remote operated vehicles (ROVs) using proper non-destructive testing (NDT) methods. As of now, many conventional NDT methods have been adopted for underwater environments with appropriate modifications, including visual inspection [2], ultrasonic testing [3], magnetic testing [4, 5], electromagnetic methods [6, 7] and radiography [8].

Although numerous methods have been employed for underwater inspections, the success of most methods largely relies on the surface condition of the object. For example, visual inspections can be compromised by surface contaminations that cover defect features; ultrasonic testing may be susceptible to wave dampening and scattering induced by surface contaminations, resulting in an inaccurate interpretation. Hence thoroughly cleaning marine growth on the surface of the object is essential for ensuring the effectiveness of most methods in routine underwater inspections. However, underwater surface cleaning, usually involving specialized equipment, skilled labor and sometimes the use of expensive cleaning agents, can be a time-consuming and costly process [9]. In addition, underwater cleaning operations when conducted by divers usually involve inherent risks and hazards such as strong currents and low visibility. Therefore, an inspection method

*Corresponding author.
Email address: zuop@artc.a-star.edu.sg (Peng Zuo)

which does not require thorough surface cleaning may provide a highly effective solution for underwater inspections.

There are only two methods capable of performing inspection without contacting the surface of the object: pulsed eddy current (PEC) and electromagnetic acoustic transducer (EMAT). In contrast to conventional eddy current method, PEC utilizes a broadband pulse rather than a single or multi-frequency excitation to energize a driver, allowing it to provide more comprehensive information about the object under inspection [10]. This method has demonstrated the ability to measure thickness with a significant lift-off distance [11] (the distance between the sensor and the surface of the object to be inspected), making it suitable for underwater inspection without removal of marine growth. However, PEC only provides relative measurement, which requires a precise calibration to ensure a high level of accuracy in the results. To achieve this, the sample used for calibration should has exactly the same condition as the object, which, nevertheless, is seldom achievable in real applications [12]. Additionally, the spatial resolution of the results decreases with an increase in the lift-off distance. Contrary to PEC, EMAT excites ultrasonic waves and calculates thickness by timing the echo, enabling it to provide absolute results with superior spatial resolution. However, EMAT is limited by poor lift-off performance, with the maximum effective lift-off distance usually smaller than 2∼3 mm [13]. This limitation renders it unsuitable for most marine growth scenarios, where the average thickness of marine growth during inspections in Europe ranges from 5 to 10 mm, or even greater in deep-sea environments, while in Southeast Asia, it is typically between 10 and 15 mm, influenced by the higher temperatures in the region [14]. Thus, EMAT is rarely employed for underwater inspection through marine growth. Considering the capability of EMAT for quantitative measurement with high spatial resolution, if the lift-off performance of EMAT can be optimized and the lift-off distance improved to at least 5 mm, EMAT may achieve a superior performance in underwater inspections under certain scenarios.

EMAT can operate based on two primary mechanism: the magnetostrictive mechanism and the Lorentz force mechanism [15, 16]. It has been reported that the magnetostrictive mechanism can achieve a higher lift-off distance. For example, a guided wave EMAT can produce longitudinal guided waves in pipes at low frequencies of 12 kHz and

20 kHz, achieving a lift-off distance of 50 mm [17]. The use of a Fe_3O_4 coating can significantly enhance the lift-off performance of EMATs, increasing the lift-off distance up to 8 mm on coated specimens [18]. However, implementing the magnetostrictive mechanism often requires surface treatment, such as introducing a magnetostrictive coating or adhesively bonding magnetostrictive foils to a specimen. This approach is impractical for many inspection cases, especially for underwater inspections with marine growth.

The aim of this paper is to propose a quantitative measurement method for underwater inspection by enhancing the lift-off performance of Lorentz force based EMAT and demonstrating its capability for quantitative thickness mapping through marine growth. This paper is organized as follows: section 2 provides a description of development of a shear wave EMAT with high lift-off performance. Section 3 investigates the lift-off performance of the developed EMAT in both air and seawater environments experimentally. Section 4 demonstrates the application of the developed EMAT for underwater quantitative thickness mapping through marine growth in laboratory conditions. Section 5 presents a discussion and section 6 summarizes the conclusions.

2. Development of shear wave EMAT with high lift-off performance

2.1. Limitation of conventional shear wave EMAT

EMAT is a noncontact transducer capable of generating and detecting ultrasonic waves in electrically conducting media. There are mainly two basic components in an EMAT: an electric coil and a permanent magnet [19]. To excite ultrasonic waves, the electric coil is driven by an alternating current (AC), which induces an eddy current in the surface of the metallic component. Followed by the coupling interaction between the eddy current and the magnetic field produced by the permanent magnet, Lorentz force is generated in the surface of the component, which acts as a source of stress within the material, creating an ultrasonic wave in the component. EMAT can also receive ultrasonic waves, accomplished by reversing the above process. The design of the magnet and the electric coil in EMATs determines the excitation of ultrasonic waves, making EMATs suitable for generating various types of waves, including bulk waves [20, 21] (shear waves and longitudinal waves) and guided waves [22, 23] (Lamb waves and Rayleigh surface waves), which therefore leads to various applications in a range of industries, such as thickness gauging [24, 25], defect inspection [26, 27] and material characterization [28]. For thickness measurement, shear wave EMAT is advantageous as the velocity of the shear wave is roughly half of the longitudinal wave for most metals and shear wave usually experiences little energy loss in underwater environments. Hence this paper focuses on the use of shear wave EMATs for thickness gauging.

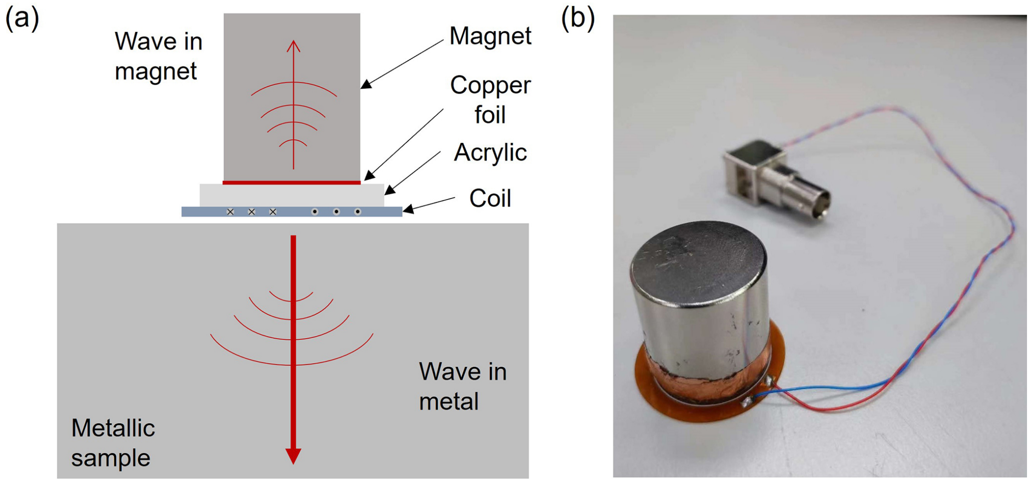

Figure 1: (a) Schematic of a conventional shear wave EMAT with pancake-like coil and (b) photo of a conventional shear wave EMAT.

Figure 1(a) shows schematic of a conventional shear wave EMAT. It consists of a flat pancake-like coil, a cylindrical permanent magnet placed right above the coil, an acrylic plate to separate the magnet and the coil and a copper film positioned at the bottom of the magnet [29]. Because of the non-contact transduction mechanism, EMAT suffers from low efficiency compared to the contact methodology, like piezoelectric transducers, which results in a weak signal, leading to a poor signal-to-noise ratio (SNR) and the performance of EMAT is sensitive to the lift-off distance. Physically, when the shear wave EMAT is moved away from a metallic sample, two major mechanisms occur. First, as the lift-off distance increases, the transduction efficiency of the EMAT decreases significantly, resulting in a lower SNR, due to the deterioration of the magnetic flux density and the eddy current induced by the coil, because both of them are inverse proportional to the lift-off distance [30]. Secondly, as the strong magnet is conductive and close to the coil, some unwanted ultrasonic signals will also be generated in the magnet. The unwanted signal, reverberating within the magnet, is then detected by the coil and introduced in the received signal, which, now working as noise, further decreases the SNR of the signal. Consequently, the signal from the sample that is used for thickness computation or defect inspection will be easily smeared out by the noise (including inherent electrical noise and unwanted signal from the magnet) when the lift-off distance exceeds a certain value.

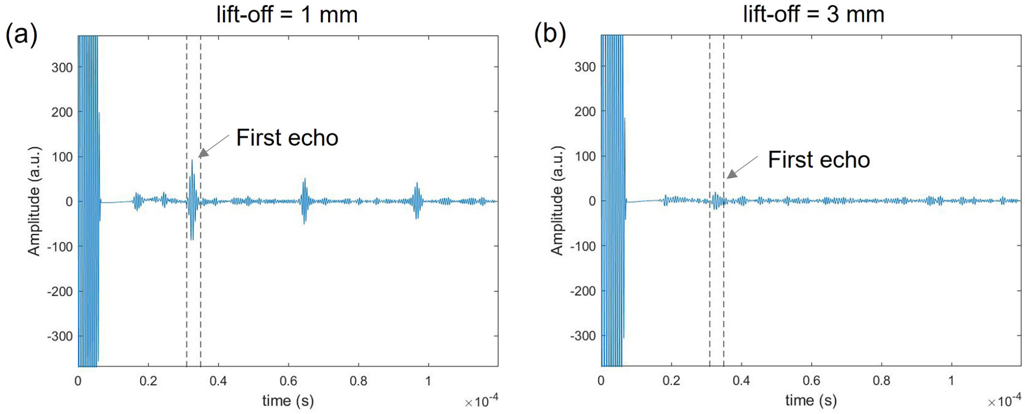

Figure 2: Signals from pulse-echo measurements on a 50 mm thick aluminum block using the conventional shear wave EMAT with lift-off distance of (a) 1 mm and (b) 3 mm. Two dashed lines indicate the location of the first echo from the metallic sample.

Figure 2 shows results of pulse-echo measurements on an aluminum block with a thickness of 50 mm using the conventional shear wave EMAT at different lift-off distances. In this context, the cylindrical permanent magnet has a diameter of 25 mm and a height of 25 mm (N52 Neodymium magnet, Supreme Magnets, Singapore), magnetized along the height direction, with surface magnetic field of approximate 6871 Gauss. The thickness of the copper foil is 0.15 mm. The acrylic plate has the same diameter as the magnet and a thickness of 3 mm. The design parameters of the coil are the same as those used in the developed EMAT shown in the next section and the setup for the experimental testing are demonstrated in Section 3.1. It can be observed that when the lift-off distance is 1 mm, the signal from the sample is significant and easily identifiable, marked by two dashed lines shown in Fig. 2(a). When the lift-off distance is increased to 3 mm, as shown in Fig. 2(b), the amplitude of the signal from the sample decreases significantly, meanwhile, the noise, consisting of electronic noise and unwanted signals from the magnet remains relatively constant. Consequently, the signal from the sample is more likely to reach the same level of the noise, leading to the signal being corrupted by the noise. Hence, conventional EMATs are usually maintained within 3 mm lift-off distance to ensure a reasonable SNR. It is important to note that the design parameters of the conventional EMAT used in the test are not optimized, thus its performance may not accurately represent that of typical EMATs.

2.2. Development of shear wave EMAT

It is clear that the key approaches to improving the performance of EMAT are to enhance transduction efficiency and minimize unwanted signals from the magnet. Although several methods have been proposed, such as employing a stronger magnet or magnetic flux concentrator [31], applying a high voltage/current to the coil (commonly operate at a voltage over a thousand volts), using laminated magnet and introducing a conductive back plate between the magnet and the coil [32], it is challenging to achieve the dual goals simultaneously. The first two methods can enhance the transduction efficiency by amplifying the signal generation in the sample, however, they also increase the signal generation in the magnet. A laminated magnet may attenuate the signals within the magnet to some extent, but they are not completely eliminated. Introducing a conductive back plate can significantly suppress the signal generation in the magnet, but the back plate may lead to a reduction in generation efficiency due to energy loss through joule heating [32].

It is interesting to note that arrangement of permanent magnets has been utilized in the past to increase the magnetic flux density for the development of medical instruments [33–35]. This arrangement can be optimized for specific magnetic fields and tailored to suit various applications. Recent publications have shown that introducing a magnet arrangement in EMATs can increase the strength of the magnetic flux thereby enhancing the transduction efficiency. For example, two permanent magnets were configured in a repelling arrangement to enhance the magnetic flux density by a factor of nearly two compared to conventional design [36]. A core-magnet arrangement has also been proposed, consisting of several magnets arranged around a ferromagnetic core. This configuration increases the magnetic field and improves the strength of the signal, with pulse-echo signals being 3$\sim$6 dB greater than those produced by conventional EMATs [37]. Even though the magnet arrangement is primarily aimed at enhancing transduction efficiency to increase the signal strength of EMATs, its great flexibility in configuration optimization suggests that a proper arrangement may achieve the dual goals of improving transduction efficiency and suppressing unwanted signals from magnets. Therefore, a generic configuration of a shear wave EMAT is proposed to improve the lift-off performance by enhancing the SNR of the signal.

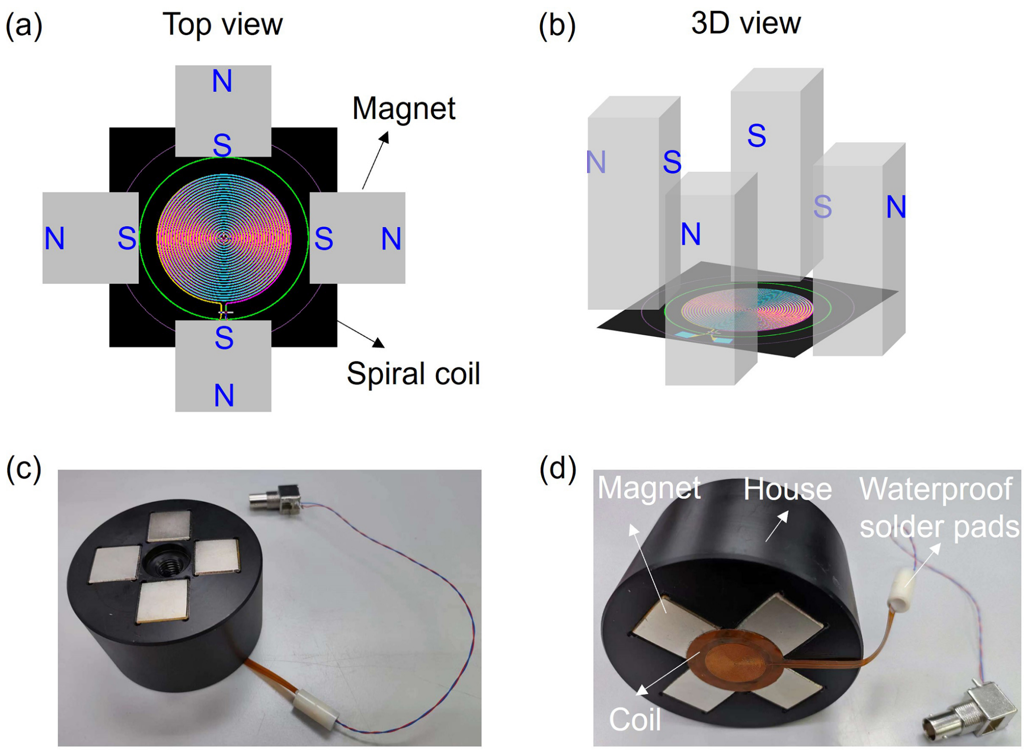

Figure 3: (a), (b) Schematic of the EMAT configuration and (c), (d) photo of the developed EMAT.

As shown in Fig. 3(a) and (b), this configuration consists of a flat pancake-like coil and a concentric arrangement of permanent magnets surrounding the coil with like poles facing each other. The magnets were encased in a cylindrical house made of derlin as shown in Fig. 3(c) and (d). The rationale behind this configuration can be understood as follows: in the arrangement, the four permanent magnets with magnetic orientation being towards the centre of the arrangement can produce an increase of magnet flux density in the space as a result of repulsion, which subsequently leads to a strong and uniform distributed normal component of the magnetic flux within this region around the coil. On the other hand, the arrangement guarantees that no conductive material is positioned above the coil, thus the ultrasonic signal is only generated on the sample when the coil is driven by an AC. Therefore, the magnets do not introduce any interference or noise into the signal. The configuration of the EMAT can greatly enhance the magnetic field as well as completely suppress the unwanted signal, thus significantly improving the SNR of the signal and thereby increasing the lift-off performance. It is worth noting that even though the configuration of magnets in this paper is similar to the core-magnet structure described in a previous study [37], the permeable core is not employed in this configuration in order to completely suppress the signal generated in the magnets, as many permeable cores, including non-conductive ferrites at high frequencies, exhibit conductivity, and additionally the purpose of the configuration is to enhance the lift-off performance rather than optimization of the bias magnetic field.

In this configuration, each of the magnets was made of Neodymium N52 with dimensions of $50\times20\times20$ mm^3 (Supreme Magnets, Singapore), magnetized through the 20 mm width with surface magnetic field of approximate 5719 Gauss. The coil is constructed using a two-layer flexible printed circuit board (PCB) by winding 22 turns of enameled wire with a width of 0.2 mm, a thickness of 1.5 ounces and wire space of 0.2 mm. This configuration results in a coil diameter of 20 mm and conveys waterproof properties to the PCB coil. In order to make waterproof solder pads, a long tail with a length of 70 mm and a width of 4 mm was incorporated into the PCB design. The solder pads were positioned at the end of the tail, and a small tube with an internal diameter of 6 mm and a length of 8 mm was utilized to cover the solder pads, filled with potting compound to completely encapsulate the solder pads, as shown in Fig. 3(d). To function the sensor, the coil was attached to the fixture and connected to a BNC connector.

3. Lift-off performance of the developed shear wave EMAT

3.1. Setup for testing

The lift-off performance of the developed shear wave EMAT was investigated in pulse-echo measurement. As shown in Fig. 4, the EMAT is connected to a pulse-echo system, which essentially consists of two Handyscopes (HS5, TiePie, Netherlands), a power amplifier (GA-25000A, Ritec Inc., USA), a diplexer (RDX-EM2, Ritec Inc., USA), an

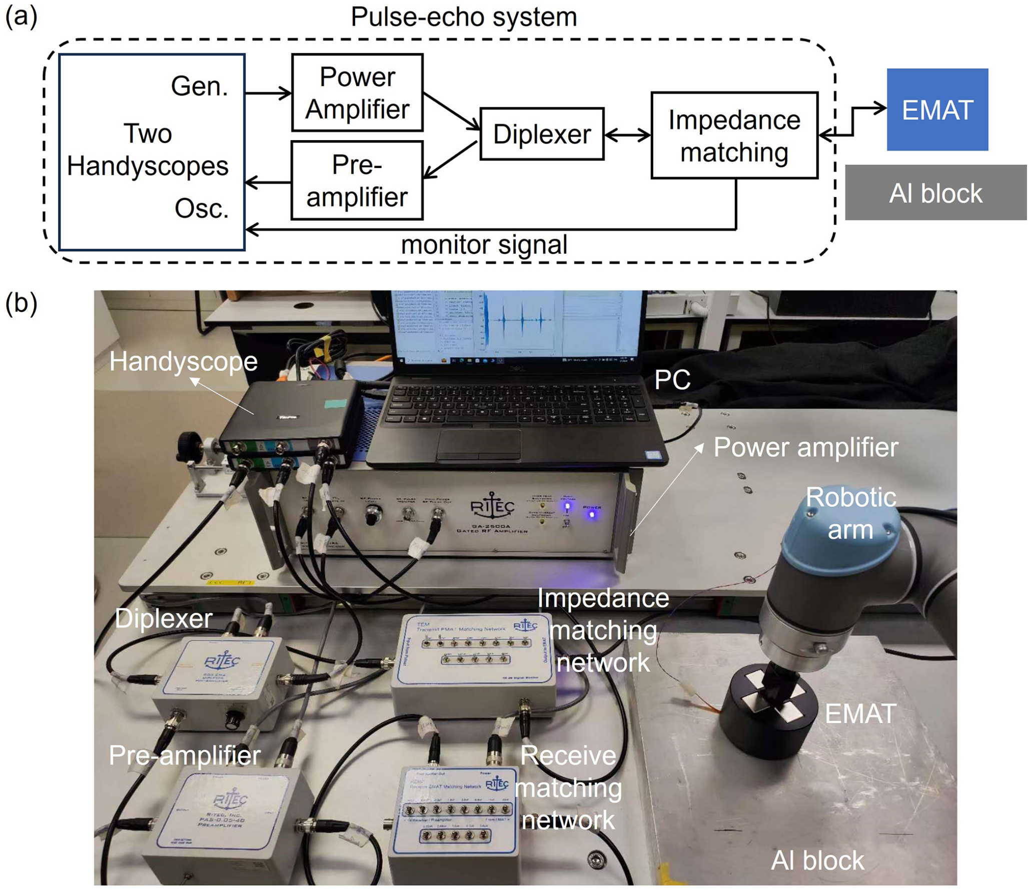

Figure 4: Experimental setup for testing the lift-off performance of EMAT. (a) Block diagram, (b) photograph of real setup.

impedance matching network (TEM-128, Ritec Inc., USA) and a pre-amplifier (PAS-0.05-40, Ritec Inc., USA). The handyscope, consisting of a programmable signal generator and a high performance oscilloscope, was employed to drive the transmitter and digitize the output of the pre-amplifier, which communicates with a PC via a USB port. The power amplifier, a wideband gated RF amplifier, was used to amplify the signal output from the function generator. The power output can be continuously adjustable through a front panel potentiometer. The diplexer allows a single EMAT to be used both for transmitting and receiving (pulse-echo mode). The impedance matching network, which consists of high voltage capacitors, that can be switched in parallel with the EMAT coil, was used to tune the impedance of the EMAT to a point where it can be more efficiently driven. The output signal of the impedance matching network was applied to the EMAT and this signal was also monitored and recorded on the oscilloscope through a -40 dB monitor port (meaning that the monitored signal is 100 times smaller than the signal applied to the EMAT), which was used for controlling the peak-to-peak voltage of the signal applied to the EMAT as well as performing cross-correlation during post-processing. It should be noted that the receive matching network was part of the system, but only the 20 dB pre-amplifier integrated into the device was utilized. The acquired signals were synchronized with the function generator and averaged in the oscilloscope to attenuate the electrical random noise. To assess the performance of the EMAT at various lift-off distances, the EMAT was mounted on a robotic arm (UR5e, Universal Robots, USA) and placed on the top of an aluminum block. The lift-off distance was adjusted by moving the robotic arm vertically along the surface of the block.

3.2. Test procedure and signal processing

The performance of the EMAT was tested on an aluminum block with dimensions of $300\times300\times50$ mm^3, as the Lorentz force mechanism is dominant in aluminum material. The tests were carried out under two conditions: in air and in seawater (artificial seawater prepared in laboratory by dissolving salts in freshwater to achieve a salinity of approximately 3.5%) for evaluating the performance of the EMAT in a normal condition and a challenging environment to understand the suitability for underwater applications. In the test, the lift-off distance of the EMAT was varied from 0 to 8 mm with a step size of 1 mm. On each lift-off distance, a 2-cycle Hann windowed tone-burst signal with central frequency of 2 MHz was generated by the function generator. The signal was amplified by the power amplifier to an amplitude of around 400 Vpp by adjusting the output power level. This relatively low voltage is used to ensure the applications of this method in oil and gas installations where the intrinsic safety regulations necessitate low power excitations. Two capacitors from the impedance matching network with capacitances of 195 pF and 410 pF were connected in parallel in the circuit to maximize power transfer. The pre-amplifier was set to 40 dB so the total gain of the system was 80 dB (40 dB is from the pre-amplifier, 20 dB is from the diplexer and the other 20 dB is from the receive matching network as shown in Fig. 4(b)). Acquired signals were synchronized for each measurement and averaged 1000 times in the oscilloscope, followed by a cross-correlation between the acquired signal and the monitored signal output from the impedance matching network. During the test, both the generator and the oscilloscope were sampled by 100 MHz. For tests in seawater, both the aluminum block and the EMAT were submerged in a water tank filled with seawater, and the sample was connected to ground, which helps minimize electrical interference in measurements by ensuring the sample and the measuring equipment share a common reference point.

To quantitatively evaluate the lift-off performance, the SNR of the signal was computed using the formula

$$SNR = 20\log_{10}(A_{signal}/A_{noise}), \tag{1}$$

where A_{signal} and A_{noise} are root mean square (RMS) amplitude of the first echo and noise, respectively. The former was calculated in a time window that covers the first echo and the latter was computed within a time window selected between the first and second echoes. The maximum effective lift-off distance of EMAT can be determined on an industry-accepted standard, typically set to be a reasonable SNR, often defined at 12 dB [18].

3.3. Lift-off performance

3.3.1. Performance in air

The experimental results for a lift-off distance of 2 mm are presented in Fig. 5. Fig. 5(a) shows the monitored signal output from the impedance matching network through the -40 dB port. As its amplitude is 100 times smaller than the signal applied to

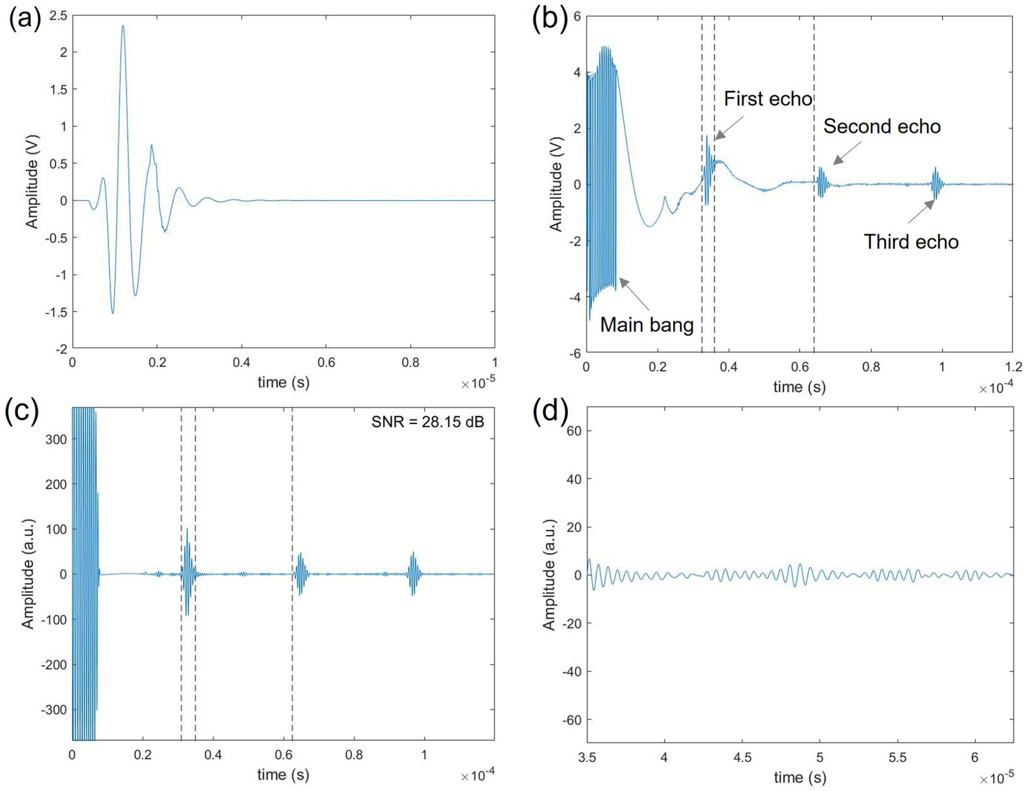

Figure 5: Signals from pulse-echo measurements using the developed EMAT with a lift-off distance of 2 mm. (a) Monitored signal output from the impedance matching network. (b) Raw received signal from the EMAT, where the first two dashed lines locate the window covering the first echo and the second and third dashed lines indicate the window between the first and second echoes. (c) Signal after the operation of cross correlation between the received signal and the monitored signal, with (d) a zoom-in of this signal between the second and third dashed lines.

the EMAT, the amplitude of the excitation signal can be computed to be approximately 400 Vpp. The raw ultrasonic signal output from the EMAT is illustrated in Fig. 5(b). A distinct main bang is observed at the beginning of the signal due to pulse-echo mode. Following this, several ultrasonic wave packets are clearly identified at different time intervals (32μs, 64μs and 96μs, respectively), corresponding to echoes reflected from the back and front walls of the block. The received signal also undergoes distortion, potentially induced by the electronics in the system, introducing low-frequency components in the signal. This received signal is subsequently correlated with the monitored signal and the resulting signal is shown in Fig. 5(c). As anticipated, the cross-correlation helps mitigate the low frequency components (distortion), emphasizing the correlated components and slightly improving the SNR. This operation is similar to the functionality of a band-pass filter commonly employed in EMAT signal post-processing. The SNR is computed using Eq. (1), where the RMS amplitude of the first echo is computed in the time window marked by the first two dashed lines in the figure, while the RMS amplitude of noise is calculated in another time window indicated by the second and third dashed lines. In this instance, the ultrasonic echo achieves a notable SNR of 28.15 dB. Fig. 5(d) displays a zoom-in of the signal between the second and third dashed lines, which illustrates the background noise. This noise exhibits a much smaller magnitude when compared to the distinct signal wave packet, showing that the background noise is practically negligible.

Figure 6 shows the received signal from the developed shear wave EMAT after the cross-correlation at various lift-off distances. It can be seen that, when the lift-off distance is nearly zero, indicating close proximity of the coil to the sample surface, the figure reveals noticeable signal distortion, leading to the amplitude of the first echo being smaller than the second echo. This distortion may be attributed to a significant change in the impedance of the system. Additionally, it is observed that the first echo amplitude decreases with increasing the lift-off distance. However, the signal can hold a notable SNR of 16.92 dB, even though the lift-off distance is increased to 5 mm, which indicates that the first echo of the signal is easily identified.

3.3.2. Performance in seawater

The testing was also carried out under seawater and the experimental results are shown in Fig. 7 for a lift-off distance of 2 mm. Similarly, the amplitude of the signal

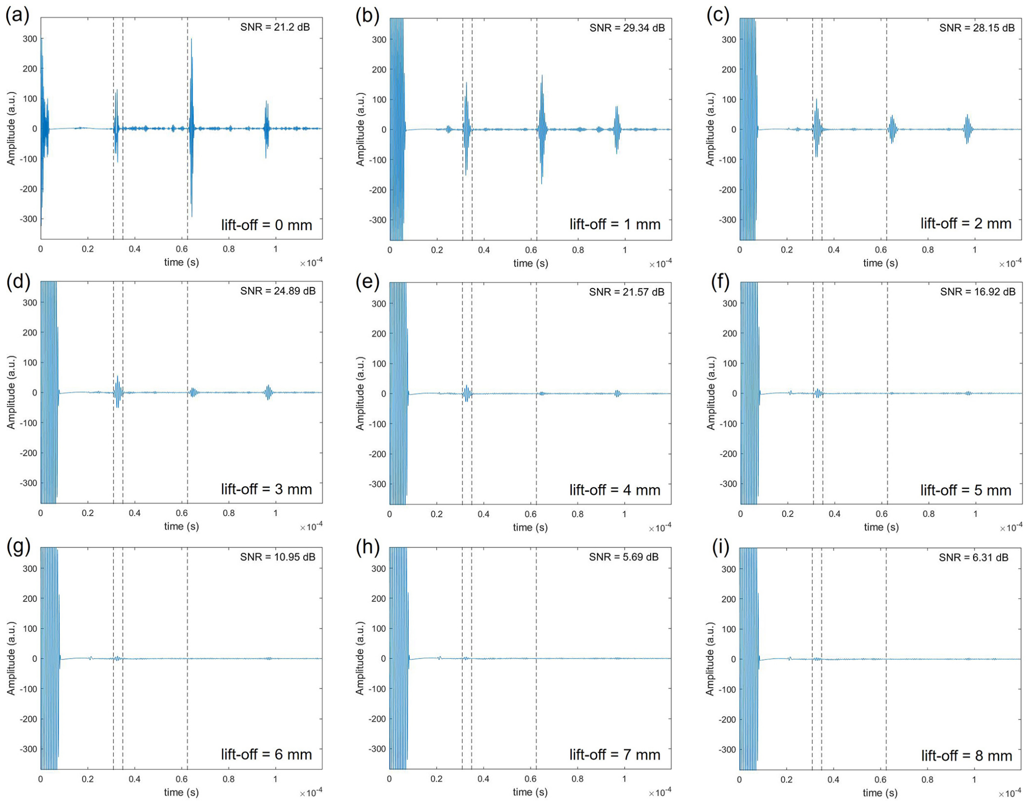

Figure 6: Signals from the developed EMAT in air condition with lift-off distance of (a) 0 mm, (b) 1 mm, (c) 2 mm, (d) 3 mm, (e) 4 mm, (f) 5 mm, (g) 6 mm, (h) 7 mm and (i) 8 mm. The first two dashed lines indicate the location of the first echo and the third dashed line show the beginning of the second echo.

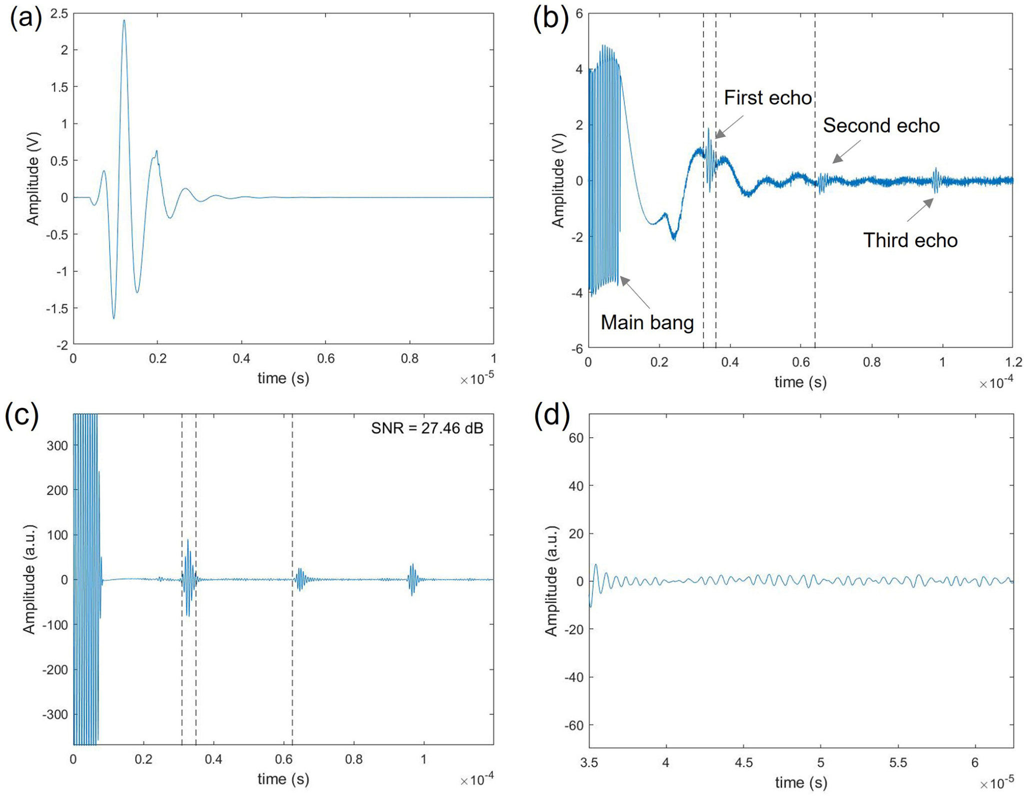

Figure 7: Signals from underwater pulse-echo measurement using the developed EMAT with a lift-off distance of 2 mm. (a) Monitored signal from the impedance matching network. (b) Raw received signal from the EMAT, where the first two dashed lines locate the first echo and the second and third indicate the region between the first and second echoes. (c) Signal after the cross-correlation, with (d) a zoom-in of this signal between the second and third dashed lines.

applied to the EMAT is around 400 Vpp, computed from the monitored signal shown in Fig. 7(a). Because of the harsh conditions in the underwater environment, more high-frequency noise can be observed in the raw received signal shown in Fig. 7(b). The cross-correlation is applied to mitigate the distortion and high frequency noise, and the result is shown in Fig. 7(c), with the signal maintaining a notable SNR of 27.46 dB. A zoom-in of the signal between the second and third dashed lines is also displayed in Fig. 7(d), showing the background noise is characterized by its extremely low amplitude, allowing the signal to dominate.

Figure 8 illustrates the time domain signal received from the developed EMAT after the cross-correlation in seawater. The EMAT displays behaviour similar to that in air, experiencing signal distortions as the lift-off distance approaches zero and achieving a notable SNR of 13.68 dB when the lift-off distance increases to 5 mm.

3.3.3. Performance comparison

The lift-off performance of the conventional EMAT, as demonstrated in Section 2.1, was evaluated and compared with that of the developed EMAT, as shown in Fig. 9. The received signals from the conventional EMAT in the time domain are not shown for the sake of brevity. It is evident that the maximum effective lift-off distance of the conventional EMAT is limited to around 2.25 mm. However, the developed EMAT demonstrates a substantial improvement, achieving up to 5.75 mm in air and 5.25 mm in the seawater condition. The slight variation in performance between air and the seawater condition may be attributed to the challenging underwater environment, which has a tendency to reduce the maximum effective lift-off distance. It is important to note that the conventional EMAT used in this paper is not optimized, and thus the observed maximum effective lift-off distance may not represent the optimal behaviour of conventional EMATs. The maximum effective lift-off distance of more than 5 mm in seawater demonstrates significant potential for underwater applications of the EMAT through marine growth.

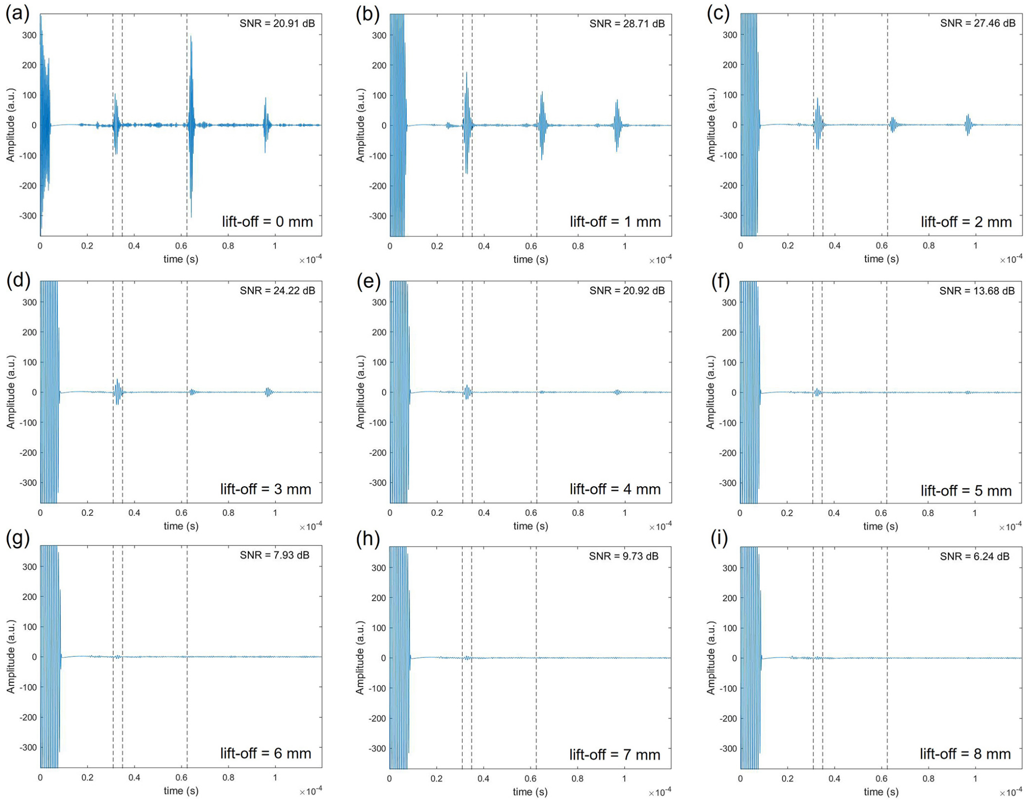

Figure 8: Signals from the developed EMAT in seawater condition with lift-off distance of (a) 0 mm, (b) 1 mm, (c) 2 mm, (d) 3 mm, (e) 4 mm, (f) 5 mm, (g) 6 mm, (h) 7 mm and (i) 8 mm. The first two dashed lines indicate the location of the first echo and the third dashed line show the beginning of the second echo.

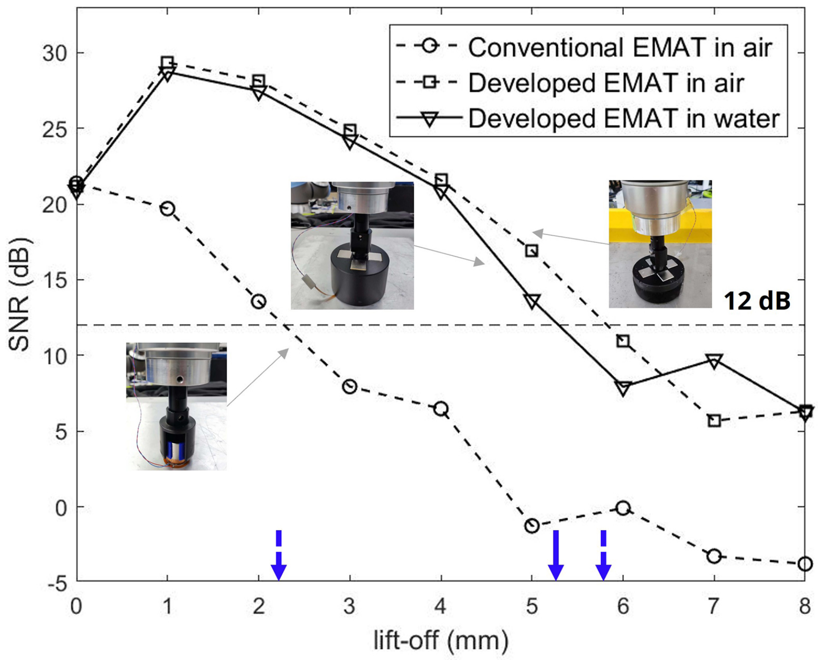

Figure 9: Lift-off performance comparison between the conventional EMAT in air condition and the developed EMAT in both air and seawater conditions. The circle, square and triangular symbols represent the performance of the conventional EMAT in air condition, the developed EMAT in air condition and this EMAT in seawater condition, respectively. The dashed line and solid line are corresponding to test in air and seawater conditions, respectively. The horizontal dashed line indicates the 12 dB threshold and the vertical downward arrows indicate the maximum effective lift-off distance for each scenario.

4. Underwater quantitative thickness mapping through marine growth

The primary objective is to quantitatively map thickness variation due to corrosion or erosion through marine growth using the developed EMAT. The thickness mapping performance of the developed EMAT in a simulated condition was therefore experimentally verified.

4.1. Sample preparation, marine growth development and scanning setup

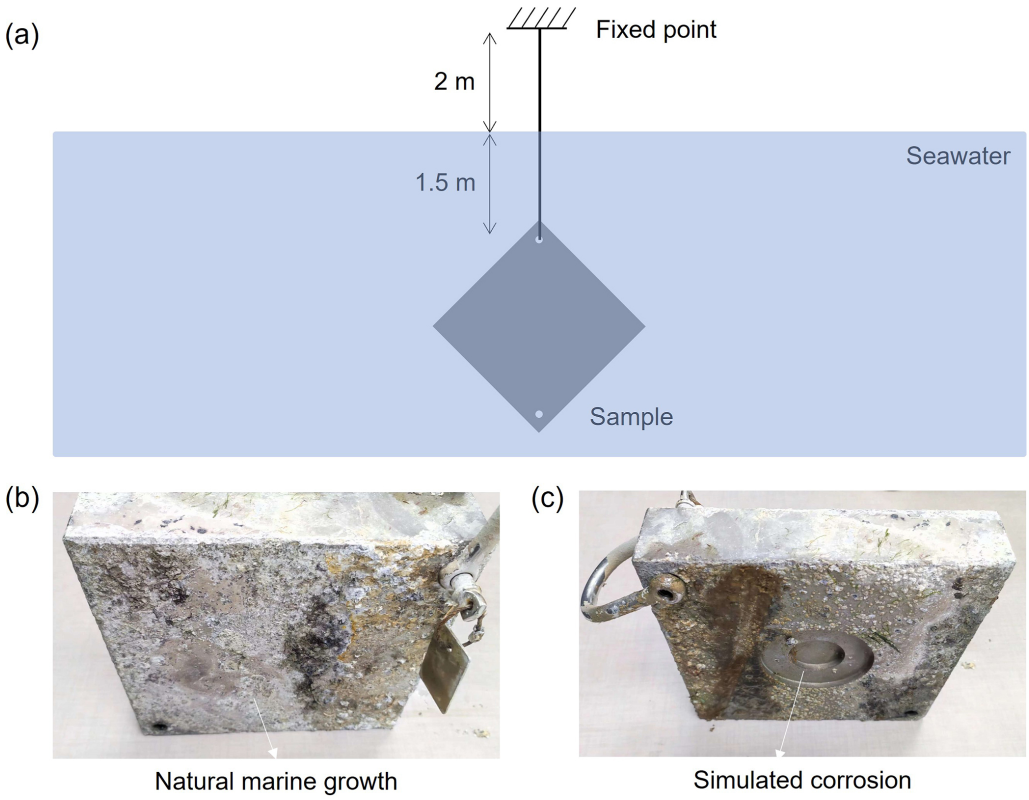

Figure 10: Natural marine growth on the sample. (a) Schematic of the seawater immersion test; (b) Front side of the sample; (c) Back side of the sample.

In the experimental validation, two pieces of aluminum block with dimension of $300\times300\times41$ mm^3 (ρ = 2700 kg/m^3, E = 69 GPa, v = 0.33) was acquired. On one side of the block, a synthetic defect was machined into the central area to simulate corrosion, which consists of two concentric circular defects: the small one with a diameter of 40 mm and a thickness of 10 mm, and the big one with a diameter of 80 mm and a thickness of 5 mm, as shown in Fig. 10(a). Two through holes with diameter of 15 mm were drilled around the two opposite corners of the block, which were used for fixing the block during the growth process of marine organism.

Testing the developed EMAT with natural marine growth can provide a realistic assessment of their performance in actual marine environments. However, the growth of marine organisms is typically a gradual process. Two types of marine growth were therefore proposed in the experiments: natural marine growth and artificial marine growth. To cultivate natural marine growth, seawater immersion tests were conducted for 60 days in Bukom island, Singapore (1°14'00"N 103°45'52"E, approximately five kilometers to the south of Mainland Singapore). The chosen location is an access-controlled area, distant from heavy anthropic activities. The sample was fixed using a long chain cable and positioned vertically at a depth of approximately 1.5 m beneath the seawater surface. Fig. 10(b) and (c) show the surface condition of the sample after the seawater immersion test. As expected, the growth of marine organism is a slow process, resulting in a thin layer of marine growth with an average thickness of 1 mm, sparsely distributed on the sample surface.

Artificial marine growth was also developed on the other sample. The preparation of artificial marine growth includes a few steps (as shown in Fig. 11): 1. smashing barnacles (removed from ship structure and provided by Tomtec NDT Marine Services Pte Ltd, Singapore) and placing them on the surface of the sample where there is no simulated corrosion; 2. using epoxy (ZS hard type epoxy resin 3:1) to adhere the smashed barnacle to the surface of the sample; 3. leaving the sample to room temperature, with a curing time of 24 hours; 4. polishing the surface of the artificial marine growth to remove any burrs and ensure a uniform thickness of approximately 3 mm. Fig. 11(b) shows the artificial marine growth on the front side of the block. Fig. 11(c) displays the back side of the block with the simulated corrosion.

To demonstrate the performance of underwater thickness mapping, the sample was placed in a water tank immersed in seawater, with the marine growth side facing upward, as shown in Fig. 12. The EMAT was mounted to the robotic arm and connected to the pulse-echo system as demonstrated in Section 3. All the parameters used in the scanning

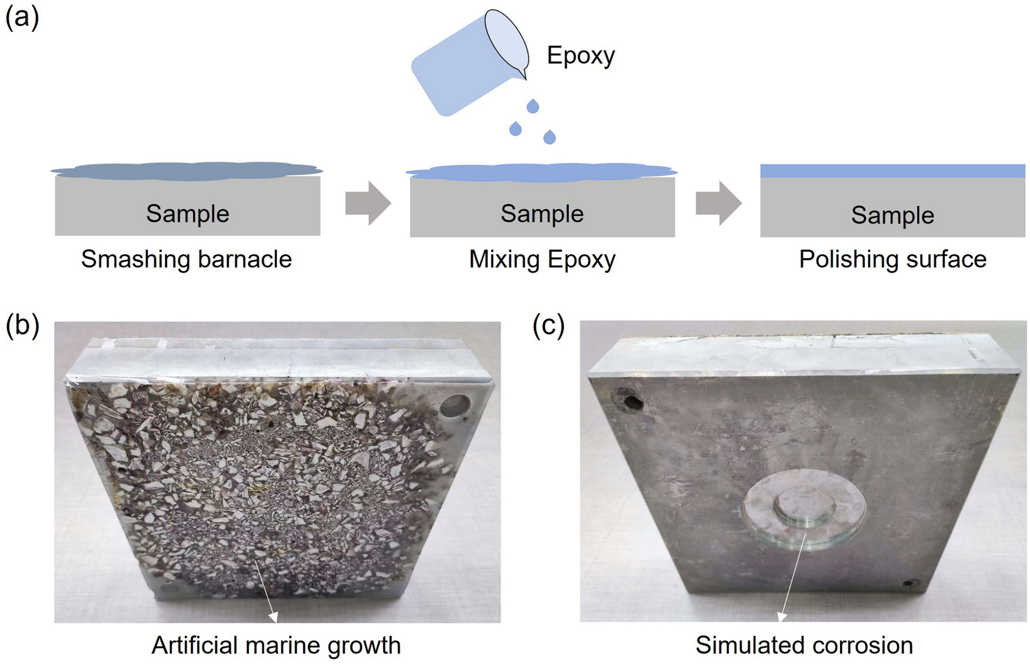

Figure 11: Artificial marine growth on the sample. (a) Schematic of artificial marine growth preparation; (b) Front side of the sample; (c) Back side of the sample.

process remained consistent with those employed in lift-off performance testing. The distance between the EMAT and the surface of the marine growth was maintained at 2 mm, therefore, the lift-off distance in the natural marine growth case is around 3 mm, and the lift-off distance in the artificial marine growth case is around 5 mm. A scanning plan was programmed to execute the C-scan, enabling the robotic arm to move the EMAT across the sample with 21×21 grid points covering an area of 120×120 mm^2 with step size of 6 mm. At each point, the EMAT excited and received ultrasonic waves in the sample, then picked up the first echo and computed the time of flight (ToF) for the first echo by searching for the peak of the wave packet. The ToF was subsequently converted into thickness based on the shear wave velocity, which was calibrated in a region with known thickness (3062.80 m/s for this sample). The thickness mapping can be displayed by linearly fitting the thickness at each point after the scanning process.

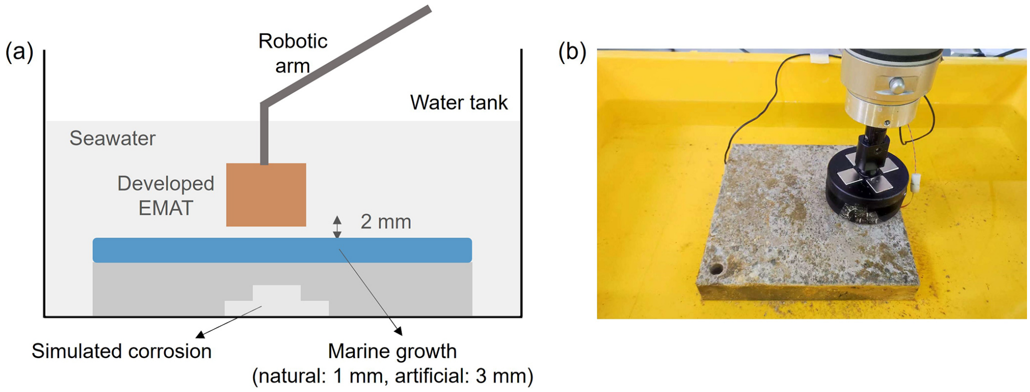

Figure 12: (a) Schematic of setup for thickness mapping through marine growth; (b) Photo of the setup with natural marine growth.

In order to assess the performance of the measurement quantitatively, two metrics were introduced [38]: the first one (referred to as error 1) is to evaluate the quality of the shape reconstruction; and the second (referred to as error 2) is to determine the accuracy of the minimum remaining wall thickness inversion. Error 1 can be calculated by

$$e1 = \sqrt{\frac{\int \left[T\left(x,y\right) - T^{*}\left(x,y\right)\right]^{2} w\left(x,y\right) \mathrm{d}x\mathrm{d}y}{T_0^2 \int w\left(x,y\right) \mathrm{d}x\mathrm{d}y}}, \tag{2}$$

where T_0 denotes the nominal thickness; $T\left(x,y\right)$ represents the measured thickness map and $T^{*}\left(x,y\right)$ corresponds to the reconstructed thickness map. w is a windowing function, determining both the extent and weighting to be applied to the error, which is defined as

$$w(r) = \begin{cases} \frac{1}{2}\left[1+\cos\left(\frac{\pi r}{A}\right)\right] & r < A \\ 0 & r \geq A \end{cases}, \quad (3)$$

where $r = \sqrt{(x-x_0)^2+(y-y_0)^2}$, with x_0 and y_0 being the location of the centre of the scanning area; A is set to be 60 mm, half of the side length of the scanning area. The window has a peak at $r = 0$ and varies smoothly down to zero at $r = A$. Error 2 is defined as

$$e2 = \frac{|T_m - T_m^*|}{T_0}, \quad (4)$$

where T_m represents the minimum thickness of the block sample, while T_m^* is the corresponding value in the reconstruction.

4.2. Thickness mapping through natural marine growth

Figure 13 presents the thickness reconstruction by using the developed EMAT through natural marine growth (shown in Fig. 13(a)-(d)) and A-scan signals (shown in Fig. 13(e) and (f)) at two representative locations, I and II, marked in Fig. 13(a). The reconstruction effectively captures key features of the defect, providing clear insights into its dimensions, geometry, thickness distribution and the location of sharp edge. Even though the sharp edge of the defect is represented by burr-like artifacts, characterized by a diffuse region around the edges, which is mainly caused by the wave scattering around the sharp edge and the relatively low spatial resolution (6 mm step size) in the scanning process, the profile of the defect and the minimum remaining thickness are accurately reconstructed with error 1 being 2.75%, signifying the successful reconstruction of the defect profile and error 2 being 0.51%, demonstrating the precise determination of the deepest point. Fig. 13(e) and (f) show the time domain signals received at locations I and II, respectively. At location I, the first echo is easily identifiable, while at location II, the first echo suffers from wave scattering around the sharp edge, which mainly causes the diffusion feature of the sharp edge observed in the reconstruction. These results demonstrate the excellent performance of the developed EMAT for underwater thickness mapping in actual marine conditions.

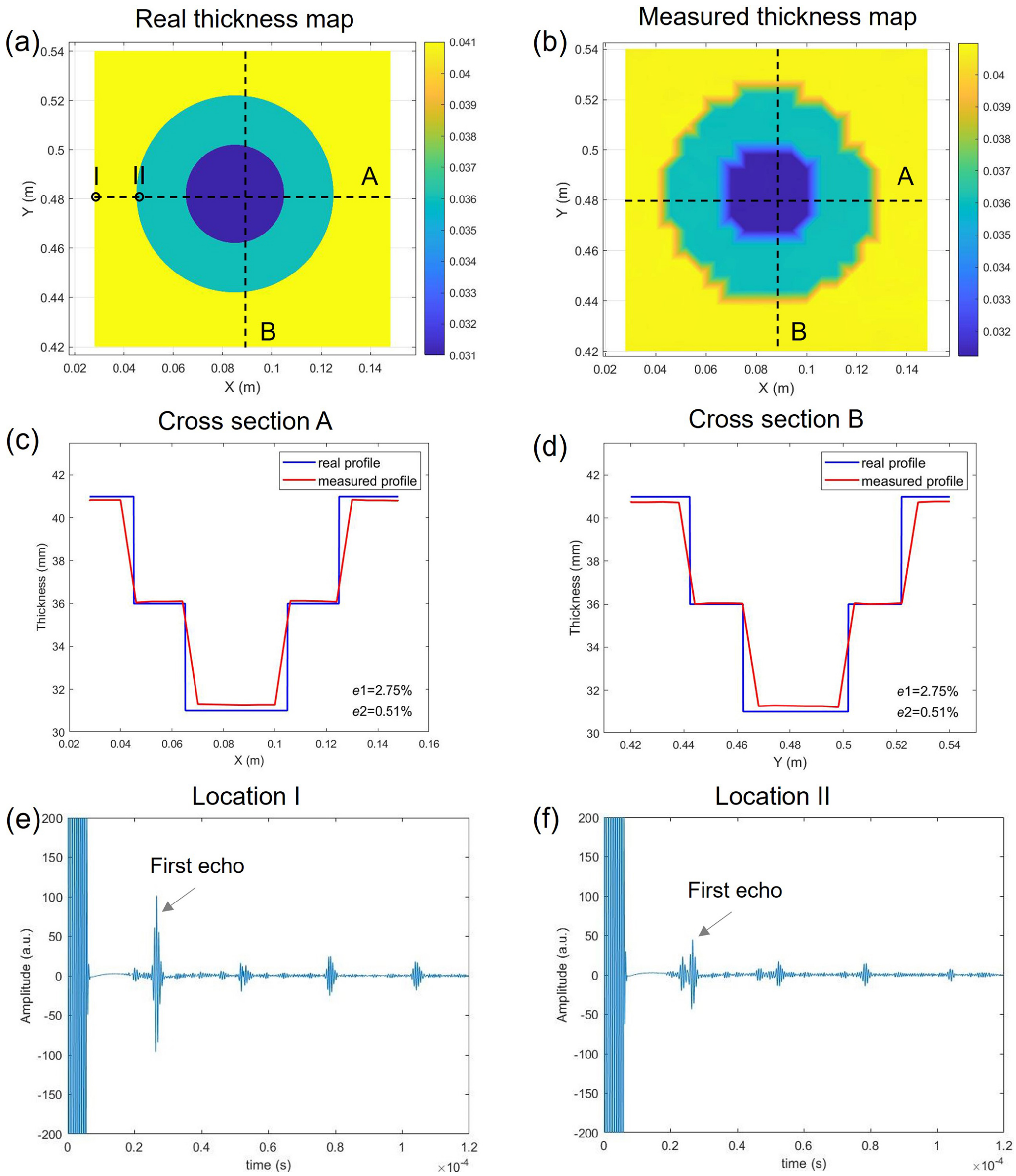

Figure 13: Reconstruction of thickness variation through natural marine growth and A-scan signals at representative locations: (a) real thickness map, (b) measured thickness map using the developed EMAT and line profile of the thickness map at (c) cross section A and (d) cross section B where e1 and e2 represent error 1 and error 2, respectively; Received signal at (e) location I and (f) location II.

.

4.3. Thickness mapping through artificial marine growth

Figure 14 displays the thickness reconstruction through artificial marine growth and A-scan signals at two representative locations. Similar to the reconstruction through natural marine growth, the developed EMAT accurately captures the dominant features of the defect, including location and dimension of the defect. However, the geometry of the sharp edge is slightly compromised in the reconstruction through artificial marine growth. This may be attributed to the rigid constraint introduced by the artificial marine growth, that could dampen the wave energy, and a relatively higher lift-off distance. Both of them may easily result in smeared signals around edges, as shown in Fig. 14(f). Nevertheless, the profile of the defect and the deepest point are well reconstructed. Error 1 is approximate 3.2% and error 2 is around 0.04%, demonstrating the superior performance of the EMAT in thickness reconstruction through artificial marine growth with a considerable lift-off distance. These results present a strong capability of the developed EMAT for underwater inspection through marine growth.

5. Discussion

It is known that the performance of EMAT is dependent on many factors, including driving voltage, magnet arrange, coil parameters [29] and post-processing. It is worth to highlight that the configuration of the developed EMAT in this paper is not optimal. Hence, there is still significant potential for further improving its lift-off performance through optimizing the design. To achieve this, additional quantitative studies on the optimal configuration of the EMAT are needed.

5.1. Driving voltage

In the test, only 400 Vpp was applied to the EMAT. Using higher exciting voltage can increase the strength of the signal, thereby enhancing the lift-off performance. Fig. 15 illustrates the lift-off performance of the developed EMAT with 600 Vpp and 800 Vpp applied. The results show that the maximum effective lift-off distance can be increased to 6.5 mm (with 600 Vpp), and 6.7 mm (with 800 Vpp) in air condition; and 5.4 mm (with 600 Vpp) and 5.7 mm (with 800 Vpp) in the seawater condition.

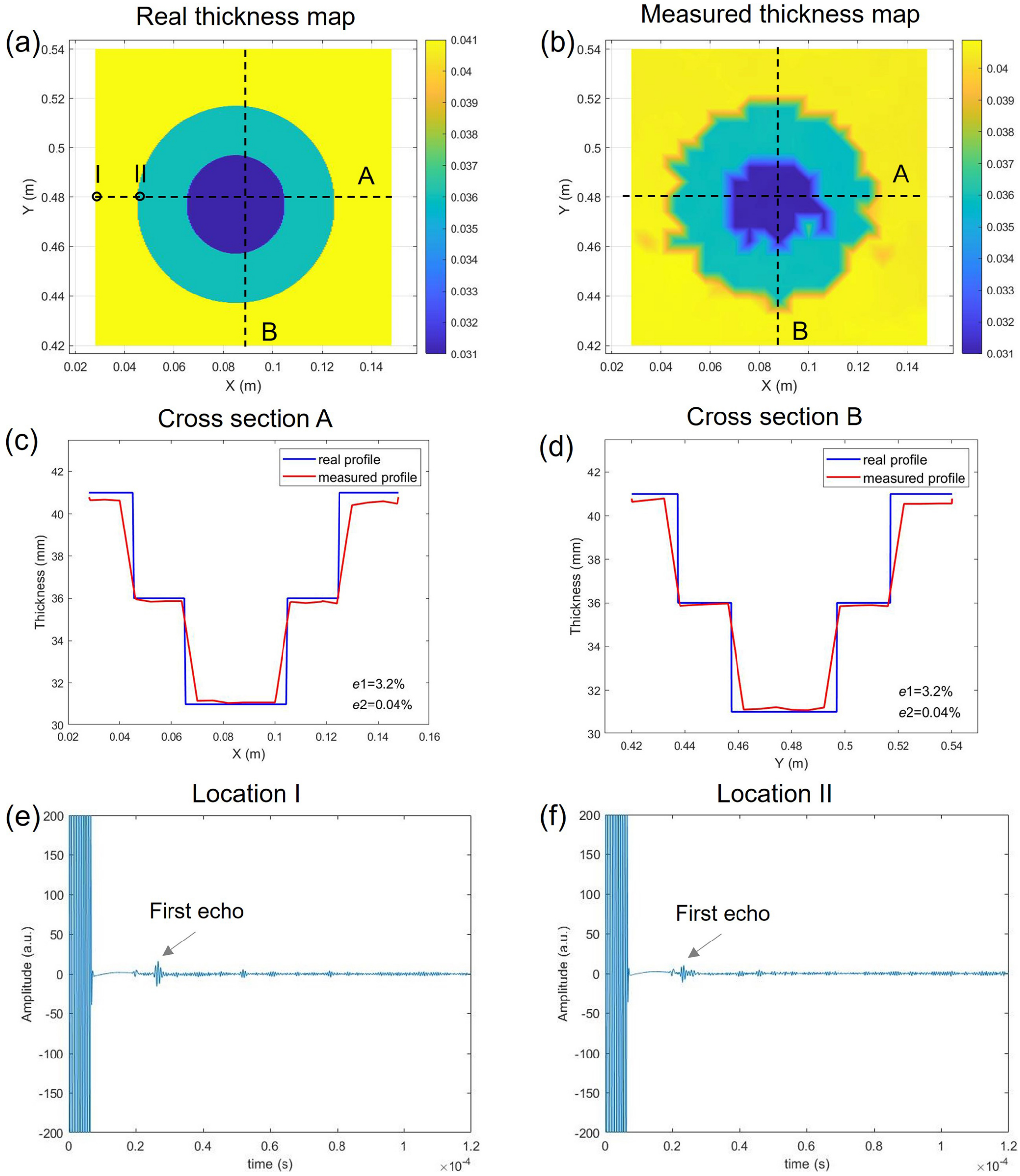

Figure 14: Reconstruction of thickness mapping through artificial marine growth and A-scan signals at representative locations: (a) real thickness map, (b) measured thickness map using the developed EMAT and line profile of the thickness map at (c) cross section A and (d) cross section B. e1 and e2 represent error 1 and error 2, respectively. Received signal at (e) location I and (f) location II.

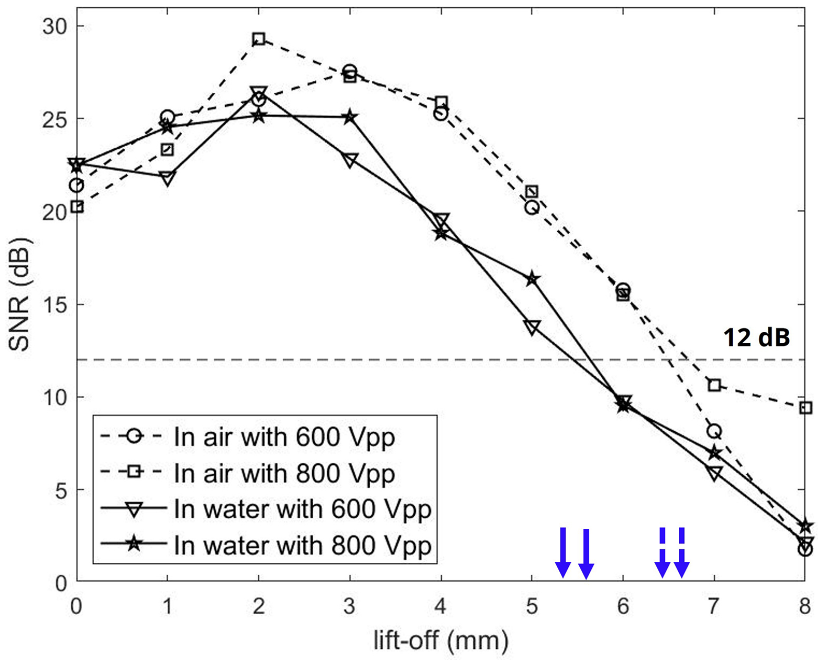

Figure 15: Lift-off performance of the developed EMAT in both air and seawater conditions. The circle and square represent the performance of the EMAT in air condition under 600 Vpp and 800 Vpp, respectively. The triangle and five star represent the performance of the EMAT in seawater condition under 600 Vpp and 800 Vpp, respectively. The dashed line and solid line are corresponding to test in air and seawater conditions, respectively. The horizontal dashed line indicates the 12 dB threshold and the vertical downward arrows indicate the maximum effective lift-off distance for each scenario.

5.2. Magnet arrangement and coil parameters

In the prototype, the repelling configuration consists of four block magnets with like poles facing each other. This configuration enhances the vertical magnetic field and ensures an even distribution. It is evident that using more magnets can further uniform the vertical magnetic field, improving the generation of pure shear waves. Therefore arc magnets and ring-shaped magnets with radial polarization may provide a more evenly distributed vertical magnetic field, leading to better lift-off performance.

The coil used in this study is unoptimized. A two-layer flexible PCB with very thin wires was employed to reduce the interference with the lift-off performance. However, the thin wires may introduce more resistance to the system, leading to increased energy consumption. It is desirable to achieve a maximum power transfer in EMAT, which is determined by the inductance of the coil, to obtain a higher SNR [39]. Hence, the parameters of the coil can be optimized, such as changing the number of turns and modifying the wire dimensions, to balance the load between the coil resistance and eddy currents, ensuring maximum power delivery to the eddy currents.

5.3. Post-processing

Increasing the averaging is straightforward to improve the SNR of the signal in post-processing. However, more averaging typically increases time consumption, making it impractical for many applications. Pulse compression has been used to increase the SNR of the signal in various applications [40–42]. This technique involves transmitting a long coded signal, capturing reflections and decoding through cross-correlation between the transmitted and received signals in order to compress signal in the time domain, thereby increasing the SNR. Employing pulse compression with the developed EMAT is another potential method to further enhance its lift-off performance, which will be studied and reported in future work.

6. Conclusion

Underwater inspection is challenged by marine growth which covers the surface of the objects to be inspected, rendering most methods impractical for quantitative measurement without the removal of marine growth. This paper presents a solution to this problem by employing a shear wave EMAT and enhancing its lift-off performance.

A shear wave EMAT, consisting of a pancake-like coil and a repelling configuration of magnets placed around the coil, is proposed, where the repelling configuration enhances the magnetic field around the coil and completely suppress the unwanted signal generated in the magnet typically occurred in conventional shear wave EMATs. This enhancement significantly improve the SNR of the signal, resulting in a substantial improvement in lift-off performance.

The lift-off performance of the EMAT was evaluated on an aluminum block under both air and seawater conditions with an exciting voltage of 400 Vpp applied to the EMAT. The results demonstrate a significant improvement in the SNR, thereby allowing for an increased maximum effective lift-off distance of up to 5 mm in both conditions.

The developed EMAT was then applied for underwater inspection to measure corrosion through natural marine growth (with a thickness of around 1 mm and a lift-off distance of 3 mm) and artificial marine growth (with a thickness of 3 mm and a lift-off distance of 5 mm). In both scenarios, the developed EMAT exhibited outstanding performance in profile reconstruction and deepest thickness inversion. The natural marine growth case indicates that the EMAT has strong capability for underwater applications in actual marine conditions. The artificial marine growth case, where the lift-off distance is around 5 mm, demonstrates huge potential for underwater quantitative thickness mapping through marine growth in certain scenarios.

In future work, the lift-off performance of the developed EMAT could be further enhanced by optimizing the configuration and incorporating pulse compression techniques. The improved lift-off performance makes the EMAT more suitable for underwater inspection through marine growth.

Acknowledgment

This research is supported by A*STAR (C222812020 and I22D1AG025). The author would like to thank Mr Edmund Ooi from Shell Singapore Pte Ltd for assistance in cultivating natural marine growth, Mr Kaixu Chia from Tomtec NDT Marine Service Pte Ltd for providing barnacle to develop artificial marine growth and Mr Yifeng Ang from ARTC, A*STAR for his assistance in the development of artificial marine growth during the experiments.

Reference

[1] P. Rizzo, Sensing solutions for assessing and monitoring underwater systems, Sens. Technol. Civ. Infrastruct (2022) 355–376.

[2] A. Khan, S. S. A. Ali, A. Anwer, S. H. Adil, F. Mériaudeau, Subsea pipeline corrosion estimation by restoring and enhancing degraded underwater images, IEEE Access 6 (2018) 40585–40601.

[3] M. Ho, S. El-Borgi, D. Patil, G. Song, Inspection and monitoring systems subsea pipelines: A review paper, Struct. Health Monit. 19 (2) (2020) 606–645.

[4] Q. Wu, K. Dong, X. Qin, Z. Hu, X. Xiong, Magnetic particle inspection: Status, advances, and challenges-demands for automatic non-destructive testing, NDT&E Int. (2023) 103030.

[5] S. Mukhopadhyay, G. Srivastava, Characterisation of metal loss defects from magnetic flux leakage signals with discrete wavelet transform, NDT&E Int. 33 (1) (2000) 57–65.

[6] M. Fan, B. Cao, A. I. Sunny, W. Li, G. Tian, B. Ye, Pulsed eddy current thickness measurement using phase features immune to liftoff effect, NDT&E Int. 86 (2017) 123–131.

[7] L. W. Yuan, Xin'an, G. Chen, X. Yin, X. Li, J. Liu, J. Zhao, J. Zhao, Visual and intelligent identification methods for defects in underwater structure using alternating current field measurement technique, IEEE Trans. Ind. Inform. 18 (6) (2021) 3853–3862.

[8] M. I. Haith, U. Ewert, S. Hohendorf, C. Bellon, A. Deresch, P. Huthwaite, M. J. Lowe, U. Zscherpel, Radiographic modelling for NDE of subsea pipelines, NDT&E Int. 86 (2017) 113–122.

[9] C. Song, W. Cui, Review of underwater ship hull cleaning technologies, J. Mar. Sci. Appl. 19 (3) (2020) 415–429.

[10] Y. Li, G. Y. Tian, A. Simm, Fast analytical modelling for pulsed eddy current evaluation, NDT&E Int. 41 (6) (2008) 477–483.

[11] Eddyfi-Technologies, Eddyfi releases lyft software version 1.1, e-Journal of Nondestructive Testing 21.

[12] F. Nafiah, M. O. Tokhi, S. Majidnia, J. Rudlin, Z. Zhao, F. Duan, Pulsed eddy current: Feature extraction enabling in-situ calibration and improved estimation for ferromagnetic application, J. Nondestruct. Eval. 39 (3) (2020) 52.

[13] P. Petcher, M. Potter, S. Dixon, A new electromagnetic acoustic transducer (EMAT) design for operation on rail, NDT&E Int. 65 (2014) 1–7.

[14] E. W. Goh, Private communication (2023).

[15] R. Ribichini, F. Cegla, P. Nagy, P. Cawley, Experimental and numerical evaluation of electromagnetic acoustic transducer performance on steel materials, NDT&E Int. 45 (1) (2012) 32–38.

[16] R. Ribichini, P. Nagy, H. Ogi, The impact of magnetostriction on the transduction of normal bias field emats, NDT&E Int. 51 (2012) 8–15.

[17] J. Xu, Z. Xu, X. Wu, Research on the lift-off effect of generating longitudinal guided waves in pipes based on magnetostrictive effect, Sensor. Actuat. A: Phys. 184 (2012) 28–33.

[18] B. Liang, Z. Li, G. Zhai, R. Yang, X. Zhang, S. Dixon, Enhancing the lift-off performance of EMATs by applying an Fe_3O_4 coating to a test specimen, IEEE Trans. Instrum. Meas. 72 (2022) 1–4.

[19] M. Hirao, H. Ogi, Electromagnetic acoustic transducers: noncontacting ultrasonic measurements using EMATs, Japan: Springer, 2017.

[20] G. Zhai, B. Liang, X. Li, Y. Ge, S. Wang, High-temperature emat with double-coil configuration generates shear and longitudinal wave modes in paramagnetic steel, NDT&E Int. 125 (2022) 102572.

[21] X. Jian, S. Dixon, I. Baillie, R. S. Edwards, J. Morrison, Y. Fan, Shear wave generation using a spiral electromagnetic acoustic transducer, Appl. Phys. Lett. 89 (24) (2006).

[22] R. Ribichini, F. Cegla, P. B. Nagy, P. Cawley, Study and comparison of different emat configurations for sh wave inspection, IEEE Trans. Ultrason. Ferroelectr. Freq. Control 58 (12) (2011) 2571–2581.

[23] Y. Xie, L. Yin, Z. Liu, P. Deng, W. Yin, A novel variable-length meander-line-coil EMAT for side lobe suppression, IEEE Sens. J. 16 (16) (2016) 6279–6287.

[24] S. Dixon, C. Edwards, S. Palmer, High accuracy non-contact ultrasonic thickness gauging of aluminium sheet using electromagnetic acoustic transducers, Ultrasonics 39 (6) (2001) 445–453.

[25] A. Thon, G. Painchaud-April, A. Le Duff, P. Bélanger, On the use of a linear array EMAT for remote thickness gauging using the reflected modes on a steel pipe, NDT&E Int. 139 (2023) 102917.

[26] R. S. Edwards, S. Dixon, X. Jian, Characterisation of defects in the railhead using ultrasonic surface waves, NDT&E Int. 39 (6) (2006) 468–475.

[27] J. Parra-Raad, B. Lan, F. Cegla, Orthogonally polarised shear waves for evaluating anisotropy and cracks in metals, NDT&E Int. 121 (2021) 102440.

[28] M. Potter, S. Dixon, C. Davis, Development of an automated non-contact ultrasonic texture measurement system for sheet metal, Meas. Sci. Technol. 15 (7) (2004) 1303.

[29] W. Shi, Y. Wu, H. Gong, T. Zhang, L. Tan, L. Han, J. Yang, W. Li, Optimal design of spiral coil electromagnetic acoustic transducers considering lift-off sensitivity operating on non-ferromagnetic media, Nondestruct. Test. Eva. 33 (1) (2018) 56–74.

[30] S. Huang, W. Zhao, Y. Zhang, S. Wang, Study on the lift-off effect of EMAT, Sensor. Actuat. A: Phys. 153 (2) (2009) 218–221.

[31] K. Mirkhani, C. Chaggares, C. Masterson, M. Jastrzebski, T. Dusatko, A. Sinclair, R. J. Shapoorabadi, A. Konrad, M. Papini, Optimal design of emat transmitters, NDT&E Int. 37 (3) (2004) 181–193.

[32] X. Jian, S. Dixon, R. Edwards, K. Quirk, I. Baillie, Effect on ultrasonic generation of a backplate in electromagnetic acoustic transducers, J. Appl. Phys. 102 (2) (2007).

[33] M. Kumada, E. I. Antokhin, Y. Iwashita, M. Aoki, E. Sugiyama, Super strong permanent dipole magnet, IEEE Trans. Appl. Supercon. 14 (2) (2004) 1287–1289.

[34] C. Li, M. Devine, Strong permanent magnet dipole with reduced demagnetizing effect, IEEE Trans. Magn. 45 (10) (2009) 4380–4383.

[35] Z. Wang, W. H. Yang, X. B. Zhang, L. L. Hu, H. X. Wang, Y. X. Zhang, Design and manufacture of a near 3 T high field permanent magnet assembly, IEEE Trans. Appl. Supercon. 22 (3) (2011) 4302304–4302304.

[36] B. Dutton, S. Boonsang, R. Dewhurst, Modelling of magnetic fields to enhance the performance of an in-plane emat for laser-generated ultrasound, Ultrasonics 44 (2006) e657–e665.

[37] J. Isla, F. Cegla, Optimization of the bias magnetic field of shear wave EMATs, IEEE Trans. Ultrason. Ferroelectr. Freq. Control 63 (8) (2016) 1148–1160.

[38] P. Zuo, P. Huthwaite, Quantitative mapping of thickness variations along a ray path using geometrical full waveform inversion and guided wave mode conversion, P. Roy. Soc. A - Math. Phy. 478 (2257) (2022) 20210602.

[39] J. Isla, M. Seher, R. Challis, F. Cegla, Optimal impedance on transmission of Lorentz force EMATs, in: AIP conference proceedings, Vol. 1706, AIP Publishing, 2016.

[40] T. Misaridis, J. A. Jensen, Use of modulated excitation signals in medical ultrasound. part i: Basic concepts and expected benefits, IEEE Trans. Ultrason. Ferroelectr. Freq. Control 52 (2) (2005) 177–191.

[41] M. P. Mienkina, C.-S. Friedrich, N. C. Gerhardt, W. G. Wilkening, M. R. Hofmann, G. Schmitz, Experimental evaluation of photoacoustic coded excitation using unipolar golay codes, IEEE Trans. Ultrason. Ferroelectr. Freq. Control 57 (7) (2010) 1583–1593.

[42] J. Isla, F. Cegla, Coded excitation for pulse-echo systems, IEEE Trans. Ultrason. Ferroelectr. Freq. Control 64 (4) (2017) 736–748.